Optical Flashes and Radio Flares in GRBs afterglow: Numerical Study

Shiho Kobayashi[1] and Re'em Sari[2]

ABSTRACT

The strong optical flash observed by ROTSE, as well as the radio flare associated with GRB 990123 can be attributed to the emission of the fireball ejecta, initially heated by the reverse shock. We numerically study the evolution of an adiabatic relativistic fireball interacting with an ambient uniform medium, both in the initial energy transfer stage and in its late evolution. It is shown that the Blandford-McKee solution adequately describes the evolution of the shocked shell quite early on and for as long as the fireball material has relativistic temperatures. In the case where the reverse shock is only mildly relativistic the shocked shell becomes cold almost immediately and the evolution deviates from the Blandford-McKee solution. We derive analytical expressions for the ejecta evolution in its cold regime. This solution gives a good approximation to the numerical results. We estimate the radiation from the fireball ejecta using the numerical hydrodynamic evolution in both cases: cold and hot shells. Surprisingly, we find that both evolutions give rather similar light curves, decaying approximately as T^{-2} in the optical and peaking at about one day in the radio, even though the hydrodynamics is different.

[1]Department of Earth and Space Science, Osaka University, Toyonaka, Osaka 560, Japan
[2]Theoretical Astrophysics 130-33, California Institute of Technology, Pasadena, CA 91125, USA

1. Introduction

Precise and prompt gamma-ray burst localization by an Italian-Dutch satellite, BeppoSAX makes it possible for other space and ground instruments to scan the same direction. The long-lasting counterparts (afterglow) in X-ray, optical and radio wavelength have been detected. Up to the event of GRB 990123, the overall behavior of the afterglows could be explained reasonably well by the synchrotron emission from the ambient medium particles (ISM) that are shocked by the relativistic flow.

GRB 990123, is the brightest gamma-ray burst seen by BeppoSAX and the fluence is in the top 0.3% of all bursts observed so far (Kippen et al. 1999). Absorption lines in the optical afterglow gave a lower limit of the redshift $z > 1.6$, the energy required to produce the bright gamma-ray burst is enormous, 3×10^{54} erg for an isotropic emission. A new clue to understand the nature of gamma-ray bursts was found in this event by ROTSE which detected a strong optical flash during the "gamma-ray" burst. ROTSE started to observe the direction in an optical band 22 seconds after the onset of the burst. The optical flash reached to a peak of 9th magnitude and then decayed with a slope of a power law index ~ 2 (Akerlof et al. 1999).

Such a strong prompt optical flash was predicted (Mészáros and Rees 1997, Sari and Piran 1999a,b). The prompt optical flash observed by ROTSE is compatible with these predictions (Sari and Piran 1999c, Mésáros and Rees 1999). In the energy transfer stage of a fireball evolution, the forward shocked ISM and the reverse shocked fireball shell carry comparable amount of internal energy. However, the typical temperature in the shocked ejecta is considerably lower than that of the shocked ISM. Consequently, the typical frequency of the synchrotron emission from the shocked shell is much lower than that from the shocked ISM, and it comes to the optical band with reasonable values of the parameters.

Beside the optical flash, GRB 990123 had another newly observed phenomenon, a radio flare (Kulkarni et al. 1999). While the usual radio afterglows rise on time scale of weeks or months, this burst had a radio flare peaking at one day, rising quickly before the peak and decaying quickly after the peak. Sari and Piran (1999c) have interpreted this flare as the emission from the ejecta particles earlier shocked by the reveres shock. The same particles producing the prompt optical flash have been cooled adiabatically and their emission shifts quickly towards lower frequencies while weakening. According to the analytical estimates of Sari and Piran, scaling the prompt optical emission to the epoch of the radio detection gives the right amount of radio emission.

The discussion of the prompt optical flush is quite robust, the estimate of the hydrodynamical evolution of the shocked ejecta is more fragile. In this paper we study numerically the energy transfer stage and the evolution of the ejecta after that in order to estimate the decay rate of the optical flash as well as the light curve and timing of the radio flare. We consider both cases, where the temperature of the shocked shell is relativistic or not. Using equipartition assumption on the magnetic field we construct the light curve of the emission from the shell. In section 2, we shortly review the hydrodynamics of a fireball. We show in section 3 the analytic estimate of the evolution of the shocked ejecta for both case of the hot and the cold shell case. The radiation from the ejecta are also estimated. In section 4, we discuss the numerical results. Finally, in section 5 we summarize the results and discuss their implications.

2. Hydrodynamics of a Fireball

The evolution of an adiabatic spherical fireball with an energy E and a dimensionless entropy (or random Lorentz factor) η and a radius R_0 is characterized by several phases (Kobayashi, Piran and Sari, 1999). Initially, the fireball expands into a surrounding medium with a low density ρ_1, a narrow shell with a radial width of $\Delta \sim R_0$ is formed. The Lorentz factor of the shell increases linearly with the radius during the free acceleration stage. At $R_L \equiv R_0\eta$ the fireball shell uses up all its initial radiation energy, it coasts with the Lorentz factor of η and the frozen radial width $\Delta \sim R_0$. The coasting ends once the ISM begins to influence the shell. The interaction between the shell and the ISM is described by two shocks: a forward shock propagating into the ISM and a reverse shock propagating into the shell.

A dimensionless quantity $\xi \equiv (l/\Delta)^{1/2}/\eta^{4/3}$ is useful to consider the evolution of the fireball shell after the coasting stage (Sari and Piran 1995) where $l \equiv (E/\rho_1 c^2)^{1/3}$ is the Sedov length. The evolution can be classified into two categories by this quantity. We call the case of $\xi > 1$ the Newtonian Reverse Shock (NRS) case, and $\xi < 1$ the Relativistic Reverse Shock (RRS) case.

If initially $\xi > 1$ (the NRS case), the coasting shell begins to spread as $\Delta \sim R/\eta^2$ at $R_s \equiv R_0\eta^2$ due to a slight difference of the velocity inside the shell. The reverse shock is initially Newtonian and becomes mildly relativistic when the reverse shock crosses the shell. After the crossing which happens at $R_\gamma \equiv l/\eta^{2/3}$, the forward shocked ISM has the most energy of the system.

If initially $\xi < 1$ (the RRS case), the reverse shock becomes relativistic at $R_N = l^{3/2}/\Delta^{1/2}\eta^2$ which is before the shock crosses the shell. At $R > R_N$ the reverse shock begins to reduce considerably the Lorentz factor of the shell's matter which it crosses. The distance between the contact discontinuity and the reverse shock is $\propto R^2$ where R is the forward shock radius. After the drastic deceleration, during the shock crossing, the shocked shell slows down as $\propto R^{-1/2}$ due to the pressure difference between the forward shock and the reverse shock. At $R_\Delta \equiv l^{3/4}\Delta^{1/4}$, the shock crosses the whole shell and most of the energy of the system has been transferred to the forward shocked ISM. The spreading effect is not important in this

case since the spreading radius R_s is larger than R_Δ.

Kobayashi, Piran and Sari (1999) have shown numerically that after R_γ for the NRS case or R_Δ for the RRS case, the profile of the shocked ISM begins to approach the Blandford-McKee solution (Blandford and McKee 1976; BM hereafter) which is the basis of most of the afterglow theories. The fraction of the energy of the ejecta rapidly decays as the forward shocked ISM has most of the energy in the system. We are interested in the evolution of this reverse shocked ejecta as the source of the rapidly decaying optical flash and the radio flare (Sari and Piran 1999c, Kulkarni et al. 1999).

3. Late Ejecta Evolution - Analytical Estimates

3.1. Hydrodynamics - Relativistic Temperatures

In the previous section we discussed the hydrodynamical evolution of the ejecta up to the time that a considerable fraction of the energy was given to the surrounding medium. Beyond this time, one has to calculate the evolution of the Lorentz factor, the pressure (or the energy density) and the mass density as functions of time in order to evaluate the emission from the ejecta. Sari and Piran (1999b,c) used the Blandford-McKee solution to estimate all these quantities. Using this solution, the Lorentz factor, the pressure and the mass density of a fluid element are given by

$$\gamma \propto R^{-7/2}, p \propto R^{-26/3}, \rho \propto R^{-13/2}. \tag{1}$$

Since the observer time is given by $T \propto R/\gamma^2 c \propto R^8$, we obtain $\gamma \propto T^{-7/16}, p \propto T^{-13/12}$ and $\rho \propto T^{-13/16}$.

Sari and Piran (1999c) found good agreement between the light curves derived with the above scalings and the observed optical flash and radio flare. However, it is not clear whether the BM solution is applicable to the reverse shocked ejecta for the following reasons. (i) The BM solution, as a self similar solution, describes the shocked ISM long after the energy transfer stage where the details of the initial conditions are no longer important. (ii) It assumes that the initial shell is irrelevant, however the evolution of that shell is what we are interested in. (iii) The initial shell contains much more particles than those collected by the forward shock. Its density therefore must be higher than that predicted by the BM solution. (iv) Though the BM solution assumes relativistic temperatures, a mildly relativistic reverse shock can not heat ejecta to such a high temperature.

It can be argued that since the shocked ejecta is located not too far behind the forward shock at the end of the energy transfer stage and it has a comparable amount of energy to that of the system, it roughly fits the BM solution. The fact that its rest mass density is much higher than that given by the BM solution should not play an important role as long as the temperature is relativistic. At relativistic temperature, the fluid inertia is due to its thermal energy rather than the rest mass. The fluid therefore can be expected to evolve according to the BM scalings with density that is higher by a constant factor from that given by the BM solution. We will show numerically that indeed the points (i)-(iii) raised above are not a real problem, and the BM solution adequately describes the evolution of the ejecta from the very early stage as long its temperature is relativistic. The forth point however, i.e., the underlying assumption of the BM solution that the temperature is relativistic might become incorrect quite early on. Specifically, if the reverse shock is only mildly relativistic, this assumption breaks from the beginning and the BM solution can not describe any of the ejecta evolution.

Mészaros and Rees (1999) assumed a general power law evolution of the forward shock and approximated

the ejecta Lorentz factor to be equal to that of the forward shock, $\gamma \propto R^{-g}$. The density was estimated by assuming that the ejecta spreads in the local frame by the speed of light, the width in the local frame is therefore R/γ. Since the number of particles there is constant, the density drops as $n \propto R^{-3}\gamma \propto R^{-3-g}$. They considered two possible evolutions of the pressure. (I) The "pressure equilibrium" assumption that the ejecta pressure is equal to the forward shock pressure, leads to $p \propto \gamma^2 \propto R^{-2g}$. (II) Adiabatic expansion $p \propto \rho^{4/3}$. In terms of observed time these scalings are: $\gamma \propto T^{-g/(1+2g)}$, $\rho \propto T^{-(3+g)/(1+2g)}$ and $p \propto T^{-2g/(1+2g)}$ for the "pressure equilibrium" and $p \propto T^{-4(3+g)/3(1+2g)}$ for the "adiabatic expansion".

Though for a larger value of g the Lorentz factor decreases faster with observed time, it is relatively insensitive to g. Even for $g \to \infty$ the Lorentz factor decreases as $T^{-1/2}$ while for the lowest reasonable value of $g = 3/2$ it decays as $T^{-3/8}$. For $g = 7/2$ one obtains the same deceleration law of the Lorentz factor and the density as a fluid element in the BM solution follows, i.e. the BM solution satisfies the spreading assumption. Furthermore, the BM solution satisfies the adiabatic expansion law, $p \propto \rho^{4/3}$, but not the pressure equilibrium. Note also that though the power law $\gamma \propto R^{-g}$ agrees with the BM evolution for a fluid element, it is not proportional to the Lorentz factor of the shock, which evolves as $R^{-3/2}$.

3.2.   Hydrodynamics - Sub-relativistic Temperatures

Non of the two papers above considered the sub-relativistic temperature regime. As mentioned earlier this regime can be important quite early on if the reverse shock is mildly relativistic. It is impossible to repeat the analysis of Sari and Piran (1999 a,b) since there is no known analytical solution describing this regime. The BM solution is not applicable since the temperature is non relativistic and the Sedov-Taylor solution is not applicable as the bulk Lorentz factor of the fluid is relativistic. However, we can minimize the uncertainty to a single parameter in a restricted range.

Assume as above that $\gamma \propto R^{-g}$. If γ is not described by a power law of R, a limited rage of radius is considered over which the value of g is approximately a constant. We can expect g to be higher than $3/2$ since the ejecta must lag behind the forward shock, but we can expect $g < 7/2$ as compared to the BM solution the ejecta has higher inertia (due to its non negligible rest mass) and therefore it is expected to be slowed down less abruptly.

We can now use a version of the spreading assumption as follows: when the ejecta arrives at radius R the time in the local frame is $R/c\gamma$. The ejecta sound speed is sub-relativistic and can be estimated by $(p/\rho)^{1/2}$. The width of the shell will therefore be $(p/\rho)^{1/2}R/c\gamma$. The ejecta density is therefore: $\rho \propto R^{-3}\gamma(\rho/p)^{1/2}$. Using the adiabatic expansion law $p \propto \rho^{4/3}$, we get

$$\gamma \propto R^{-g}, p \propto R^{-8(3+g)/7}, \rho \propto R^{-6(3+g)/7}. \tag{2}$$

In terms of the observer time these scalings become: $\gamma \propto T^{-g/(1+2g)}$, $p \propto T^{-8(3+g)/7(1+2g)}$ and $\rho \propto T^{-6(3+g)/7(1+2g)}$.

We note that the above derivation is not rigorous. A power law evolution of γ as function of radius is not necessarily correct in the sub-relativistic temperature regime. Moreover, the spreading assumption may not be valid if the pressure gradients in the ejecta are steep. We therefore use the above only as a guiding line to compare with the numerical results.

We assumed above (and through the paper) that the fluid is described by a constant adiabatic index $\hat{\gamma} = 4/3$. This is clearly true as long as the protons are relativistic. Once the shell is cold and the protons

are no longer relativistic, their adiabatic index becomes $\hat{\gamma} = 5/3$. A mixture of newtonian protons and relativistic electron results in adiabatic index of $\hat{\gamma} = 13/9$ if the two species are kept in equipartition. However, the basic assumption here is that some level of equipartition is only created by the passage of a shock since the collision time is too long. Once the proton become newtonian and their adiabatic index becomes $\hat{\gamma} = 5/3$, electrons and protons will deviate from equipartition since they evolve differently. They always have the same density due to the charge neutrality but the thermal energy of protons evolves as $\rho^{5/3}$ while that of the electrons evolves as $\rho^{4/3}$. As ρ decreases, the relativistic electrons dominate the thermal energy and the pressure of the fluid. Since the electrons are still relativistic far after the protons become cold we assume that the fluid is described by a constant adiabatic index $\hat{\gamma} = 4/3$, even after the shell become cold with newtonian protons.

3.3. The Ejecta Emission

The reverse shock propagates into the shell and heats its electrons. After it has crossed the shell, no new electrons are injected. The emission from the reverse shocked shell reaches the peak at R_γ for a NRS case ($\xi > 1$) or R_Δ for a RRS case ($\xi < 1$). Since the Lorentz factor of the shocked region at that time is η and $\xi^{3/4}\eta$ respectively, the peak time for the observer is given by $\xi^2 R_0/c$ and R_0/c respectively. According to the internal shock model the duration of the gamma-ray burst itself is R_0/c.

After the peak time when the reverse shock crossed the shell, the shocked electrons cool radiatively and adiabatically. We consider here the simplest case in which the energy of the magnetic field remains a constant fraction of the internal energy $B^2 \propto p$. The electron random Lorentz factor evolves as $\gamma_m \propto p/\rho$ due to the adiabatic expansion. The typical synchrotron frequency in the observer frame is $\nu_m \propto \gamma\gamma_m^2 B$, the spectral power at the typical frequency is $F_{\nu_m} \propto \gamma B$ for a fixed total number of radiating electrons. Assuming a power law distribution of the electron random Lorentz factor with index $\hat{p}$, the spectral flux at a given frequency above ν_m is $F_\nu \sim F_{\nu_m}(\nu/\nu_m)^{-(\hat{p}-1)/2}$ while below ν_m we have the synchrotron low energy tail as $F_\nu \sim F_{\nu_m}(\nu/\nu_m)^{1/3}$. Substituting the expressions for ν_m and F_{ν_m} we have

$$F_\nu \propto \begin{cases} \gamma^{2/3}p^{-1/3}\rho^{2/3} & \nu < \nu_m \\ \gamma^{(\hat{p}+1)/2}p^{(5\hat{p}-3)/4}\rho^{-(\hat{p}-1)} & \nu > \nu_m. \end{cases} \tag{3}$$

This is a generalized form of equation 3 in Sari and Piran (1999c) in which they substituted the BM relations and $\hat{p} = 2.5$ to get a $T^{-2.1}$ decay above ν_m and a $T^{-17/36}$ below ν_m.

If the power law scalings (2) are valid, typical frequency ν_m and the peak flux F_{ν_m} evolve as $\nu_m \propto T^{-3(8+5g)/7(1+2g)}$ and $F_{\nu_m} \propto T^{-(12+11g)/7(1+2g)}$. The flux at a frequency below ν_m (above ν_m) drops as $T^{-2(2+3g)/7(1+2g)}$ ($T^{-(7+24\hat{p}+15\hat{p}g)/14(1+2g)}$). These decay indexes of the flux are monotonic functions of g and are not so sensitive to it. If the value of g is limited as $3/2 < g < 7/2$, these vary in relatively narrow rages for $\hat{p} = 2.5$. The index for the low frequency part is between -0.46 and -0.44, the index for the high part is between -2.2 and -1.8. These are very close to the estimates from the BM scalings.

At low frequencies and early times, self absorption takes an important role and significantly reduces the flux. A simple estimate of the maximal flux is the emission from the black body with the reverse shock temperature. The temperature is given by the random energy of the typical electron $m_e c^2 \gamma_m$ for a frequency below the typical frequency ν_m. If the observed radio frequency is above it, the electron radiating into the observed frequency has energy higher by a factor $(\nu/\nu_m)^{1/2}$ since the synchrotron emission frequency is proportional to the square of the Lorentz factor. Using the same expression as in Sari and Piran (1999c),

but leaving arbitrary the hydrodynamic evolution we get an upper limit to the emission of

$$F_\nu \cong 5.0 \times 10^{-8} [\text{Jy}] \gamma^3 \gamma_e \max \left[1, \left(\frac{\nu}{\nu_m} \right)^{1/2} \right] \left(\frac{T}{1\text{day}} \right)^2 \left(\frac{\nu}{8.5 \text{ GHz}} \right)^2. \tag{4}$$

where we assumed $\Omega_0 = 1, \lambda_0 = 0$, $h = 0.65$ and the location of the fireball $z = 1.6$ as GRB990123. The emission will therefore be the minimum between that given by equation (3) and equation (4).

Since our numerical simulation is purely hydrodynamic, we can not use them to verify any of the radiation assumptions leading to equations (3) and (4). We will therefore use the above expression to evaluate the output radiation from the hydrodynamical properties of the ejecta. However, we will be able to get a more realistic hydrodynamic by using the numerical simulations.

4. Numerical Simulation

The initial configuration for our simulation is a static uniform spherical fireball surrounded by a uniform cold ISM. It is determined by four parameters: the total energy E, the dimensionless entropy η, the initial radius R_0 and the ISM density ρ_1. E and ρ_1 always appear as the ratio of E/ρ_1 in the hydrodynamics computation, the system is actually determined by three parameters, the initial radius R_0, the entropy η and the Sedov length l. First we consider two extreme cases: of the RRS $\xi << 1$ and the NRS $\xi >> 1$ to see the difference clearly. Then, the case of GRB 990123 will be studied.

4.1. the Relativistic Reverse Shock Case

The temperature of the reverse shocked ejecta is one of the differences between the RRS case and the NRS case. We suspect that the relativistic temperature is a crucial condition to apply the BM solution to the shocked ejecta. We consider a relativistic reverse shock case $E = 3 \times 10^{54}$erg, $\rho_1 = 10$ proton cm^{-3}, $\eta = 2 \times 10^5$ and $R_0 = 3 \times 10^{10}$cm, and we compare the evolution of the ejecta with the BM solution. This parameter set corresponds to $\xi = 10^{-3}$.

For computational efficiency, this simulation is started at $R_\Delta/100 \sim 5 \times 10^{14}$ cm at which the ejecta shell is in the coasting stage. It is larger than $R_N \sim 2 \times 10^{12}$ cm where the reverse shock becomes relativistic, but at that time only 10^{-6} of the ISM material within R_Δ had been swept up. In other word, the reverse shock had decelerated 10^{-4} of the shell (Sari and Piran 1995; Kobayashi, Piran and Sari 1999). Therefore, the deceleration prior to this time can be neglect.

Initially, the unshocked fireball shell has all the energy of the system. As the shell expands, the reverse shock decelerates the ejecta while the forward shock accelerate the ISM. The energy is transferred from the unshocked shell to the ISM via the shocks, finally the shocked ISM carries all the energy of the system. In the intermediate stage, around R_Δ, the shocked shell has comparable energy to the shocked ISM. The evolutions of the energies in three regions, inside of the reverse shock (unshocked shell), between the reverse shock and the contact discontinuity (shocked shell) and between the contact discontinuity and the forward shock (shocked ISM) are shown in figure 1.

We numerically define the reverse shock crossing time $R_{\Delta,num}$ as the time at which the energy in the shocked shell becomes equal to the unshocked one. $R_{\Delta,num}$ is $\sim 3.3 \times 10^{16} \sim 0.7R_\Delta$ cm in this case. The profile at $R_{\Delta,num}$ is plotted in figure 2, we can clearly see the forward and the reverse shock and the contact

discontinuity. The widths of the shocked ISM and the shocked fireball are comparable, the analytical estimate is $\sim R_0/2 = 1.5 \times 10^{10}$cm.

The Lorentz factor of the shocked shell is about 700 which is comparable to the analytic estimate $\xi^{3/4}\eta \sim 1100$. There is a gap of the density at the contact discontinuity while pressure is almost constant through the shocked regions, then the random Lorentz factors (or the temperature) e/ρ are different in the two shocked regions separated by the discontinuity. The numerical values are about 100 in the reverse shocked and 700 in the forward shocked while the analytic estimates is $\xi^{-3/4} \sim 180$ and $\xi^{3/4}\eta \sim 1100$, respectively.

In the BM solution, the Lorentz factor, the density and the pressure are given by

$$\gamma/\gamma_2 = \chi^{-1/2}, p/p_2 = \chi^{-17/12}, \rho/\rho_2 = \chi^{-5/4}, \tag{5}$$

where γ_2, p_2 and ρ_2 are the values of the Lorentz factor, the pressure and the density just behind the forward shock and the similarity variable χ is defined by $\chi \equiv 1 + 16\gamma_2^2(t)(1 - r/R(t))$ with the shock radius $R(t)$. Radius r and time in the observer's rest frame t are independent coordinates here. After the reverse shock crossed the shell at $\sim R_{\Delta,num}$, a rarefaction wave begins to propagate from the inner edge of the shell, crosses the contact discontinuity and continues towards the forward shock. Around $2R_{\Delta,num}$, it reaches the forward shock, the separation between the contact discontinuity and the forward shock becomes comparable with the thickness of the blast wave $R/4\gamma_2^2$. Then, the profile of the forward shocked region approaches to the BM solution. The profile normalized by the value just behind the forward shock at different times are plotted in figure 3. The boundaries of the ejecta shell are indicated by the filled and the open circles. The former is the contact discontinuity, the latter marks the fluid element in which the reverse shock has been at time $R_{\Delta,num}$.

The profile of the reverse shocked ejecta except the density one (the right side of the filled circle) also approaches to the BM. This can be understand as follows, since the temperature of the shocked ejecta is relativistic, the internal energy dominates the fluid inertia. The density gap at the contact discontinuity is negligible for the evolution of the ejecta since its inertia is given by its internal energy rather than its rest mass and the BM solution fits the profile. The evolution of the Lorentz factor, the pressure and the density of the ejecta shell are plotted in Figure 4. After the rarefaction wave reaches the forward shock around $2R_{\Delta,num}$, the scalings of the ejecta are also adequately approximated by the BM scalings for a fluid element.

We define the effective scaling indexes, $-R/\gamma \cdot d\gamma/dR$, $-R/p \cdot dp/dR$ and $-R/\rho \cdot d\rho/dR$. The evolutions of the averaged values in the shocked shell are plotted against the radius of the forward shock in figure 5. The scaling index of the Lorentz factor g is about 3 in stead of 7/2 of the BM solution, after the rarefaction wave reaches the forward shock. The dotted lines depict the analytic estimate (2) assuming the numerical index g. The analytic estimate fits the numerical results as long as the bulk motion is relativistic, the spreading assumption and the adiabatic expansion law are therefore good approximation.

4.2.   the Newtonian Reverse Shock Case

We consider the other extreme case in which the shocked ejecta is cold from the beginning. The initial condition is $E = 3 \times 10^{54}$erg, $\rho_1 = 10$ proton cm^{-3}, $\eta = 10^3$ and $R_0 = 3 \times 10^7$cm. This corresponds to the NRS case of $\xi = 44$.

In the NRS case, the energy of the ejecta is transferred to the ISM when the forward shock collects

ISM mass of E/η^2 around $R_\gamma \sim 6 \times 10^{16}$ cm. The reverse shock crosses the ejecta at the same time. The numerical estimate is $R_{\Delta,num} \sim 3 \times 10^{16}$cm.

The Lorentz factors of the shocked regions are about 700 at that time. The reverse shocked ejecta is already cold $3p/\rho \sim 0.05$ while the forward shocked ISM is hot $3p/\rho \sim 700$. The profiles at different times are plotted against the similarity variable χ in figure 6. At $\sim 2R_{\Delta,num}$ the forward shocked region is relatively well described by the BM scaling, but there is a break at the contact discontinuity and the reverse shocked region deviates from it. The reverse shock does not heat the shell well, the pressure of the shocked region is less than the value expected from the BM solution. The evolution of χ_e for a fixed element in the BM solution is given by $\chi_e = \chi_{e0}(R/R_0)^4$ where R_0 and χ_{e0} are the initial shock radius and the initial value of χ. At $R_{\Delta,num}$, the boundaries of the shell are at $\chi = 2.5$ and 2.7, the analytic formula gives that the values are 40 and 43 at $2R_{\Delta,num}$, 203 and 219 at $3R_{\Delta,num}$. However, the shocked ejecta departs from the forward shock slower, the numerical correspondences are 4.5 and 4.6 at $2R_{\Delta,num}$, 8.3 and 8.4 at $3R_{\Delta,num}$.

The profile of the shocked regions does not deviate from the self similar scalings so much in figure 6, but the evolution of χ_e is much slower. The hydrodynamic variables of the shocked shell evolve slower. In figure 7 the averaged values of the Lorentz factor, the pressure and the density in the shell are compared with the BM solution (equations 1). Though the values just behind the forward shock (thin solid line) fit the BM scalings well around $2R_{\Delta,num}$, the numerical scaling (thick solid line) is very different from the BM one for a fluid element. The effective scaling index of γ is about 2.2 as we can see in fig 8. The analytic estimates (2) based on the spreading assumption and the adiabatic expansion are good approximation as long as the bulk motion is relativistic.

4.3.   GRB 990123

We have seen the two extreme cases: the RRS ($\xi << 1$) and the NRS ($\xi >> 1$). In the RRS case the BM solution can describe well the evolution of the shocked ejecta, but the scalings of the NRS are very different from the BM. The fireball of GRB 990123 is actually a marginal case as we see soon. However, such marginal cases behave very much like the NRS as the shell becomes cold at the early stage.

According to the internal shocks model the duration of the gamma-ray burst is determined by the thickness of the relativistic flow which is the initial fireball size. The T_{90} duration of GRB 990123 is 63 sec in the 50-300keV range (Galama et al. 1999). The burst profile is dominated by two peaks, each lasting 8 sec, separated by 12 sec, we assume $R_0/c = 40$ sec. The observations suggest that the typical synchrotron frequency of the reverse shock is below the optical bands quite early on, then the initial Lorentz factor of the ejecta is a few hundred (Sari and Piran 1999c). $\eta = 400$ is assumed here. The explosion energy and the ambient density are rather ambiguous. We assume $E = 1 \times 10^{54}$ergs and $\rho_1 = 5$ protons cm^{-3}. This is a marginal case of $\xi = 0.7$.

The explosion energy might be higher since the internal shocks can not convert the whole kinetic energy of the flow into the thermal energy and that only some part of thermal energy goes into random motions of the electrons (Kobayashi, Piran and Sari 1997). However, the sedov length determining the hydrodynamic time scale are relatively insensitive to E. A non-spherical (jet) geometry of the ejecta are suspected from the break in the afterglow light curve (Kulkarni et al., 1999). Even in this case, a spherical fireball simulation is still valid to study the energy transfer stage due to relativistic beaming.

When the reverse shock crosses the ejecta around $R_{\Delta,num} \sim 8.4 \times 10^{16}cm \sim 0.9R_\Delta$, The Lorentz

factor of the shocked regions is about 120. The reverse shocked regions is already cold from the beginning $e/\rho \sim 0.6$ while the forward shocked region is hot $e/\rho \sim 120$. The temperature ratio is ~ 200 close to the analytic estimate $\eta\xi^{3/4} \sim 300$.

At $\sim 2R_{\Delta,num}$ the forward shocked region is well described by the BM scaling (see fig 9), the reverse shocked region deviates from it. The reverse shock does not heat the shell as well as in the RRS case. At $R_{\Delta,num}$, the boundaries of the shell are at $\chi = 2.5$ and 3.4, the analytic formula gives that the values are 40 and 54 at $2R_{\Delta,num}$, 203 and 275 at $3R_{\Delta,num}$. The numerical correspondences are 5.2 and 6.8 at $2R_{\Delta,num}$, 16 and 19 at $3R_{\Delta,num}$, considerably smaller.

The hydrodynamic variables of the shocked shell evolve slower than the BM (see 10). The vertical dotted lines show the time when the Lorentz factor of the ejecta shell becomes $\gamma = 5$ and $\gamma = 2$. These happen at 0.55 day and 6.2 day respectively for the observer. The effective scaling index of γ is about 2.2 which is the same to that of the NRS case (see fig 11). The analytic estimates (2) are good approximation again as long as the bulk motion is relativistic.

The optical flash of GRB 990123 initially decayed as T^{-2}. This implies that the typical synchrotron frequency is already below the optical band at the peak, we use the high frequency part ($\nu > \nu_m$) of the equation 3 to estimate the optical flash. Using a normalization 1.7 Jy at the peak and the numerical evolutions of γ, p and ρ, the optical light curve is plotted in figure 12. The ROTSE observations are also plotted (stars), the arrows mean the upper limits. This normalization value of 1.7 Jy is double of the second ROTSE observation 0.81 Jy, it gives good fits to both of the optical flash and the radio flare. The normalization is actually done at the radio flare.

The steepness of the light curve is about -2 at late time with a steeper slope at early times. The numerical light curve reasonably fits the observation (see figure 12), the numerical light cure also qualitatively shows a steeper initial decline where the rarefaction wave is going through the shell. The deviation can be due to some reasons. The second observation of ROTSE has been assumed to be just at the peak, but the observation is sparse and the exposure duration is 5 sec. It is also possible that the real peak is in between the second (47 sec) and the third (72 sec) ROTSE data. This will allow the higher peak value. A more fundamental problem is that in internal shocks model, the source is not a single explosion. At the end of the internal shock phase (GRB phase) we are left with rather ordered flow in which faster ejecta are the outermost ones and slower follow behind them. At the afterglow phase the outermost ones are decelerated by the ISM, the slower ones collide into them. This effect makes the decay of the light curve slower (Panaitescu, Mészaros and Rees 1998).

Emission from the reverse shock can also explain the radio flare, the radio detection one day after the burst (Sari and Piran 1999c, Kulkarni et al. 1999). The shocked ejecta initially radiates in the optical band. As the ejecta expands, the temperature of the ejecta becomes lower. The emission frequency and the flux drop quickly, eventually the emission comes to the radio band and further lower.

We use the same normalization with the optical flash estimate, the flux of 1.7 Jy at the typical frequency $\nu_m = 5 \times 10^{14}$ Hz at 52 sec. The peak frequency $\nu_m \propto \gamma p^{5/2}\rho^{-2}$ reaches 8.5GHz after 12 hours, the peak flux $F_{\nu_m} \propto \gamma p^{1/2}$ is 1.5 mJy at that time. After that the flux at the radio band drops as $\propto \gamma^{(\hat{p}+1)/2}p^{(5\hat{p}-3)/4}\rho^{-(\hat{p}-1)}$. The flux at 8.5 GHz is plotted in figure 13.

Self absorption can reduce the radio flux. Using equation 4 with $\epsilon_e = 0.6$ (Granot, Piran and Sari 1998), the upper limit is numerically estimated (dotted dashed line in fig 13). When accounting for this, the resulting emission is the minimum between the solid line and the dotted dashed line. The estimates

fit very well to the radio observation. Since the emission is normalized with the observation, only the evolution scalings of the hydrodynamic variables are important to estimate it. On the other hand, the self absorption estimate 4 depends on the absolute values. It is relatively sensitive to the Lorentz factor and the temperature of the ejecta.

5. Discussion

We have studied numerically the evolution of fireballs. Specifically we focused on the evolution of the reverse shocked ejecta which is causing the optical flash and the radio flare of GRB990123. We have seen that the Blandford-Mckee solution is not applicable to the shocked ejecta in a NRS case in which the reverse shock is Newtonian or mildly relativistic and the temperature of the shocked ejecta is not relativistic. However, in a RRS case in which the reverse shock is relativistic, the profile of the reverse shocked ejecta as well as the forward shocked ISM approached to the solution after the reverse shock had crossed the ejecta. The self similar solution is rigorous only after the details of the initial conditions becomes no longer important. We find that initially a steeper decline may be expected, qualitatively compatible with the observations of GRB 990123.

The hydrodynamics of the cold shocked ejecta are very different from that of the hot shocked ejecta which is well described by the Blandford-Mckee solution. The numerical scaling relations for a cold one were well approximated by the spreading assumption and the adiabatic expansion law, while the Blandford-Mckee solution satisfies the relativistic version of it. We have estimated the radiation from the fireball ejecta in both cases: cold and hot shells. Surprisingly, we find that both evolutions give rather similar light curves even though the hydrodynamics is very different.

After the reverse shock crossed the ejecta shell, the electrons cools due to the adiabatic expansion, the emission frequency and the flux drop quickly. The radio flare, the single radio detection one day after the burst is the late time correspondence to the early optical flash. Using the numerical results we have shown that the reverse shock can explain the radio flare observation a day after the burst, in agreement with the previous analytical estimates.

The late time afterglow is less sensitive to the property of the original ejecta, which is determined by only one parameters, the ratio between the explosion energy and the density of the ambient medium. The new observation window, the optical flash is very useful to probe the original ejecta and ultimately the inner engine producing it. Future optical flash and radio flare observations will enable us to know about the original ejecta more. Numerical simulations similar to the one presented here will be useful for the detailed study.

References
Akerlof, C.W. et al. 1999, GCN 205.
Blandford,R.D. & McKee,C.F. 1976, Phys. of Fluids, 19, 1130.
Fenimore,E.E., Ramirez-Ruiz, E. and Wu, B. 1999, astro-ph/9902007.
Galama, T.J., 1998, astro-ph/9804191.

Galama, T.J., 1999, astro-ph/9903021.

Granot,J., Piran,T. & Sari,R. 1998, astro-ph/9808007.

Kippen, R.M. et al., GCN, 224.

Kobayashi,S., Piran,T. & Sari,R. 1997, ApJ, 490, 92.

Kobayashi,S., Piran,T. & Sari,R. 1999, ApJ, 513, 669.

Kulkarni, S.R., et al., Nature, submitted, astro-ph/9902272.

Mészaros,P. & Rees,M.J. 1997, ApJ, 476, 231.

Mészaros,P. & Rees,M.J. 1999, MNRAS, submitted,astro-ph/9902367.

Panaitescu,A., Mészaros,P. & Rees,M.J. 1998, ApJ, 503, 314.

Sari,R. & Piran,T. 1995, ApJL, 455, 143.

Sari,R. & Piran,T. 1997, ApJ, 485, 270.

Sari,R. & Piran,T. 1999a, A&A, in press, astro-ph/9901105.

Sari,R. & Piran,T. 1999b, ApJ, in press, astro-ph/9901338.

Sari,R. & Piran,T. 1999c, ApJL, in press, astro-ph/9902009.
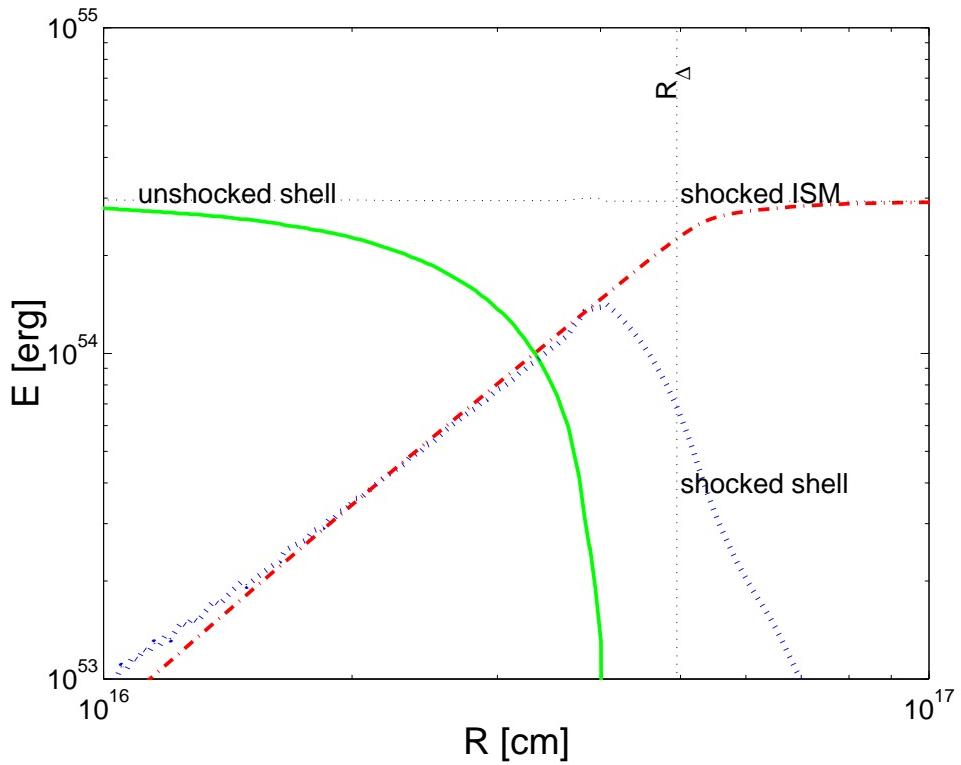
Fig. 1.— Energy transfer from the fireball to the shocked regions. The sum of the kinetic and the thermal energies in the unshocked shell (solid line), in the reverse shocked shell (dotted line) and in the forward shocked ISM (dashed dotted line). The horizontal dotted line is the sum of the energies in the three region. R_Δ (vertical dotted line) is a analytic estimate where the reverse shock crosses the ejecta.
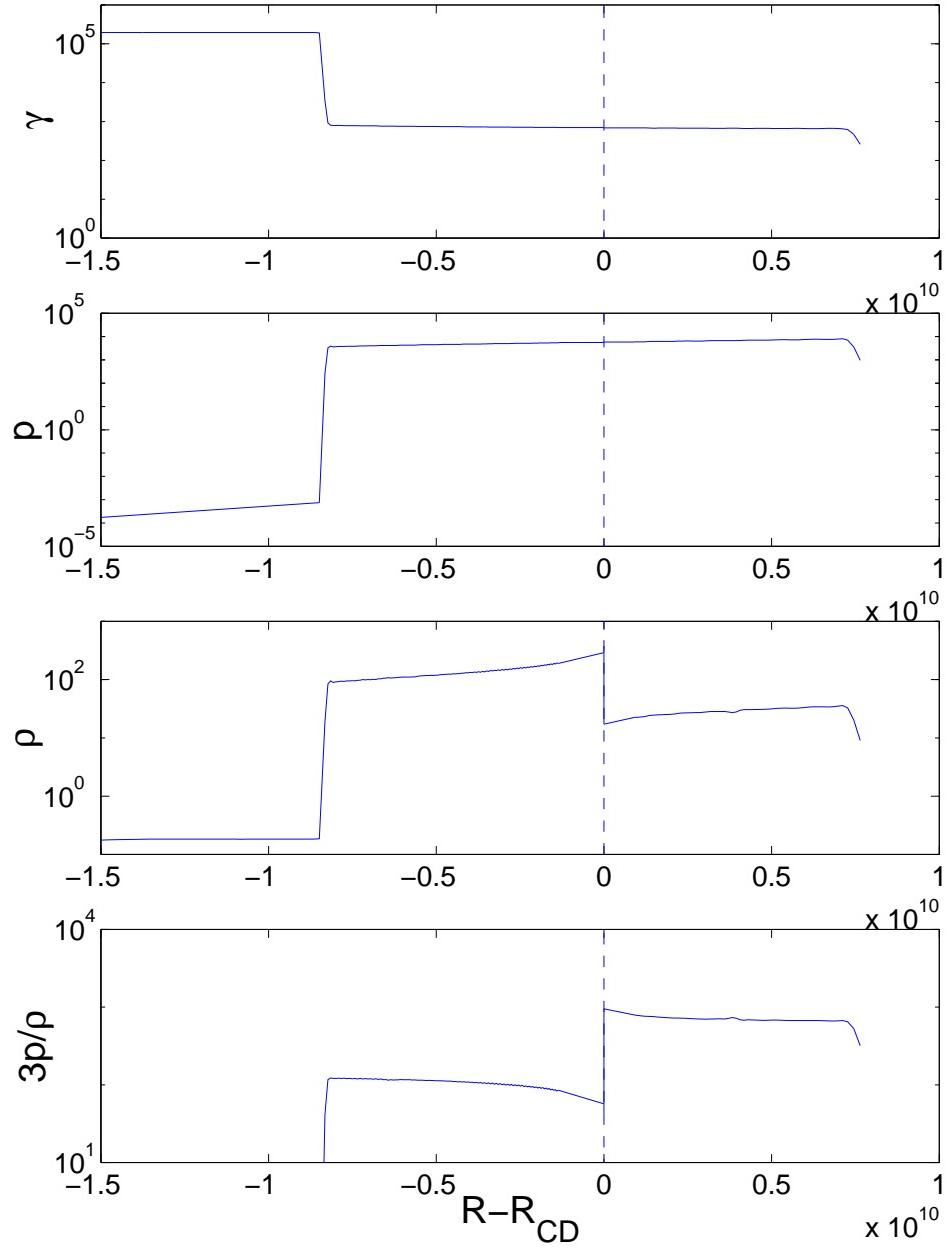
Fig. 2.— Profile: Lorentz factor, pressure, density and random Lorentz factor at the crossing time, $R_{\Delta,num}$. The x-axis is the distance from the contact discontinuity.
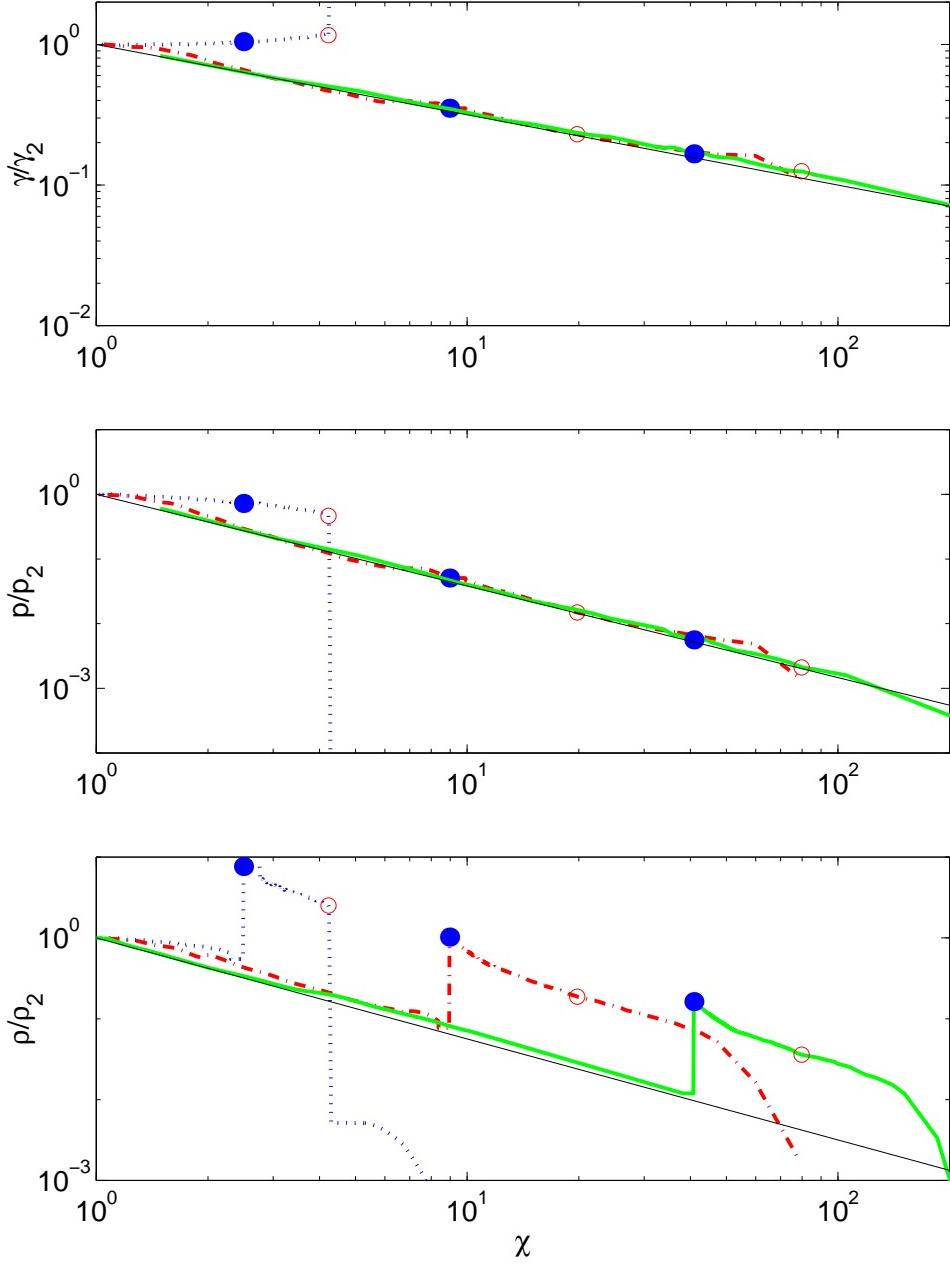
Fig. 3.— RRS case: Lorentz factor, pressure and density as functions of χ at $R_{\Delta,num}$ (dotted lines), at $2R_{\Delta,num}$ (dotted dashed lines) and at $3R_{\Delta,num}$ (solid lines). The Blandford-McKee solution is the thin solid lines. The ejecta shell is bounded by the contact discontinuity (filled circle) and the fluid element where the reverse shock is at $R_{\Delta,num}$ (open circle). γ, p and ρ are normalized with γ_2, p_2 and ρ_2 which are numerical values just behind the forward shock.
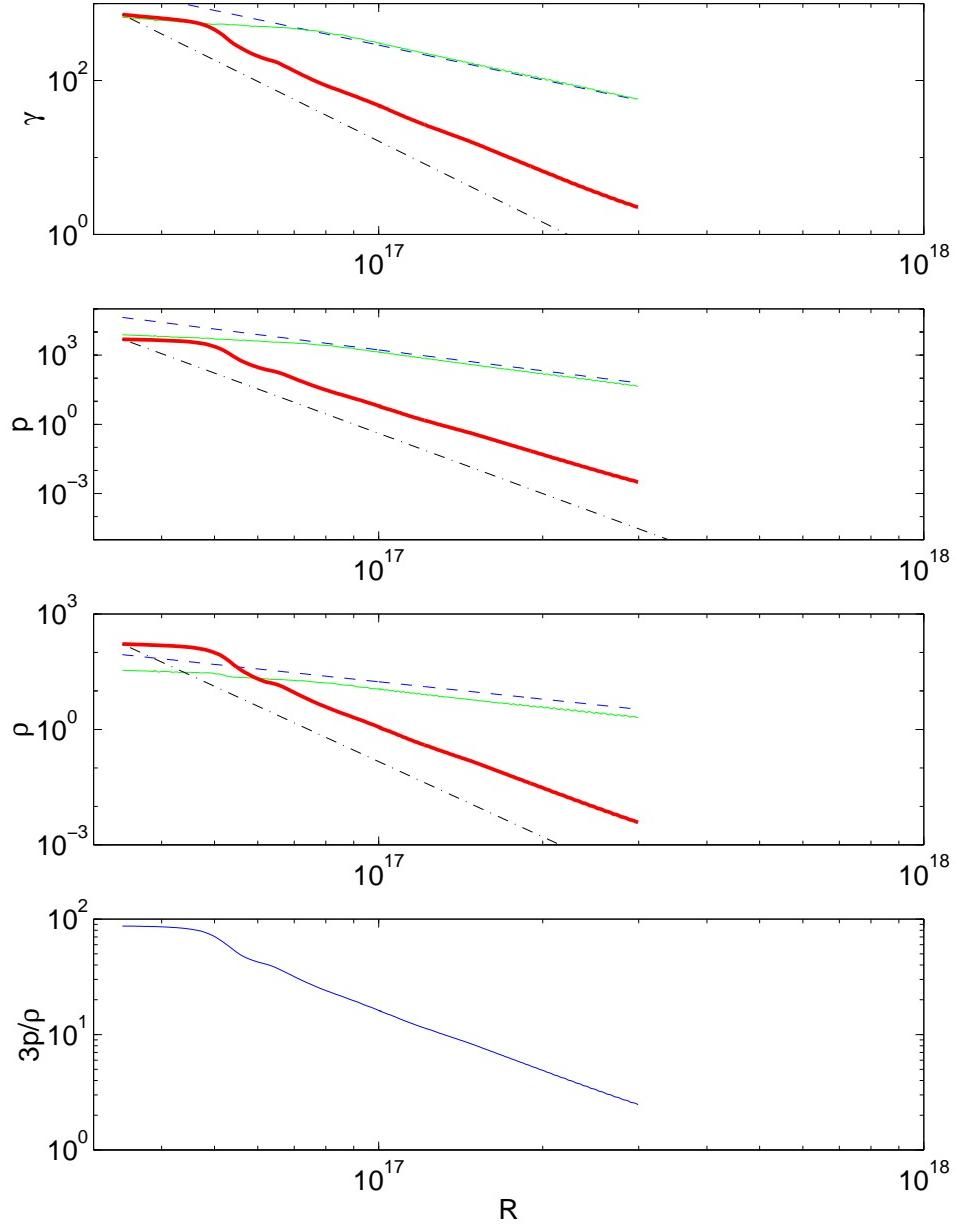
Fig. 4.— Evolution of Lorentz factor, pressure and density: RRS case. The numerical values just behind the forward shock are the thin solid lines, the expected values from the Blandford-McKee solution are the thin dashed lines. The numerical evolution of the averaged values in the ejecta shell (thick solid lines) are compared with the Blandford-McKee scalings of a fluid element (thin dashed dotted lines).
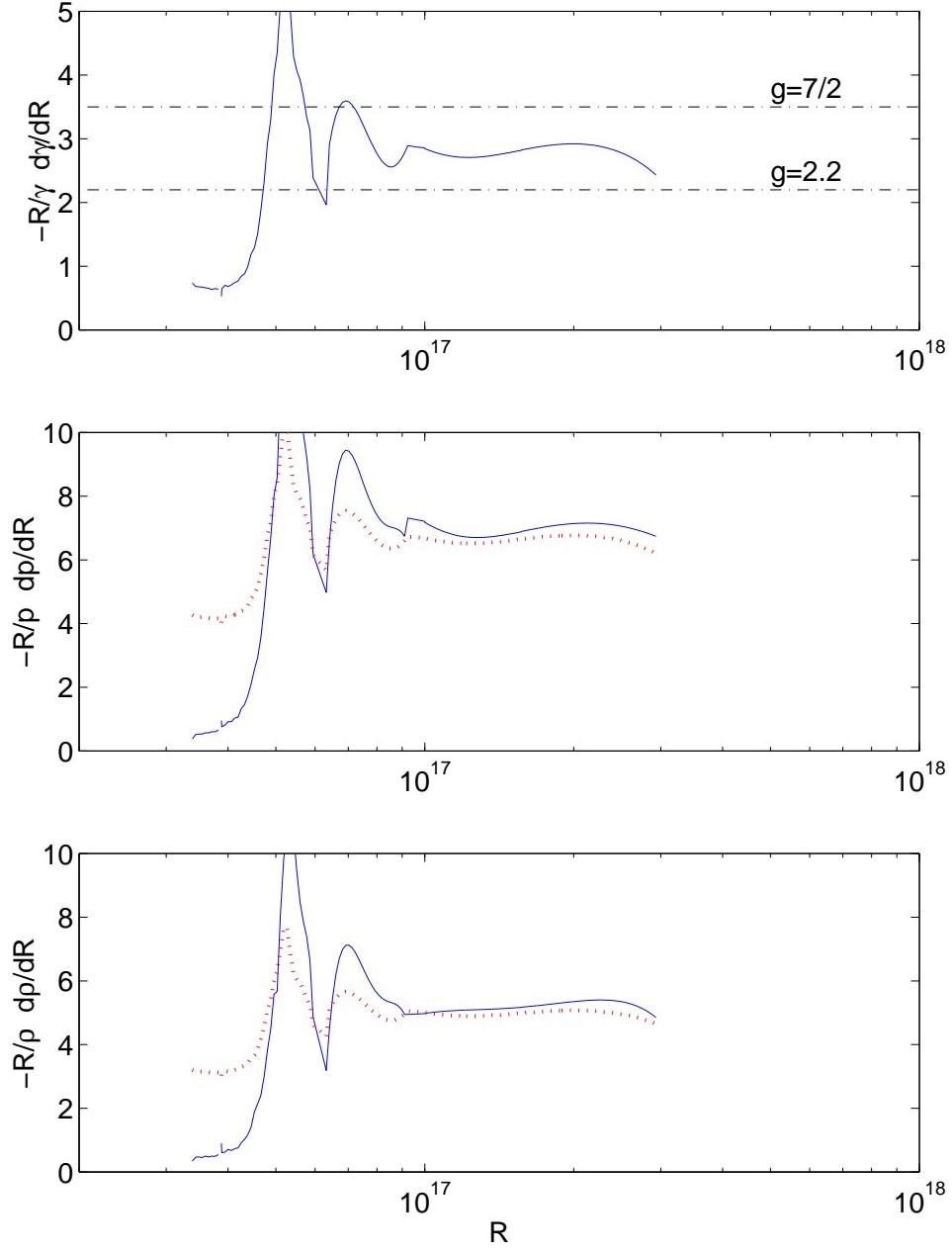
Fig. 5.— Effective scaling indexes vs Radius of the shell: RRS case. The numerical results are the solid lines. The dotted lines in the middle and the bottom panel are analytic estimates assuming the numerical index g.
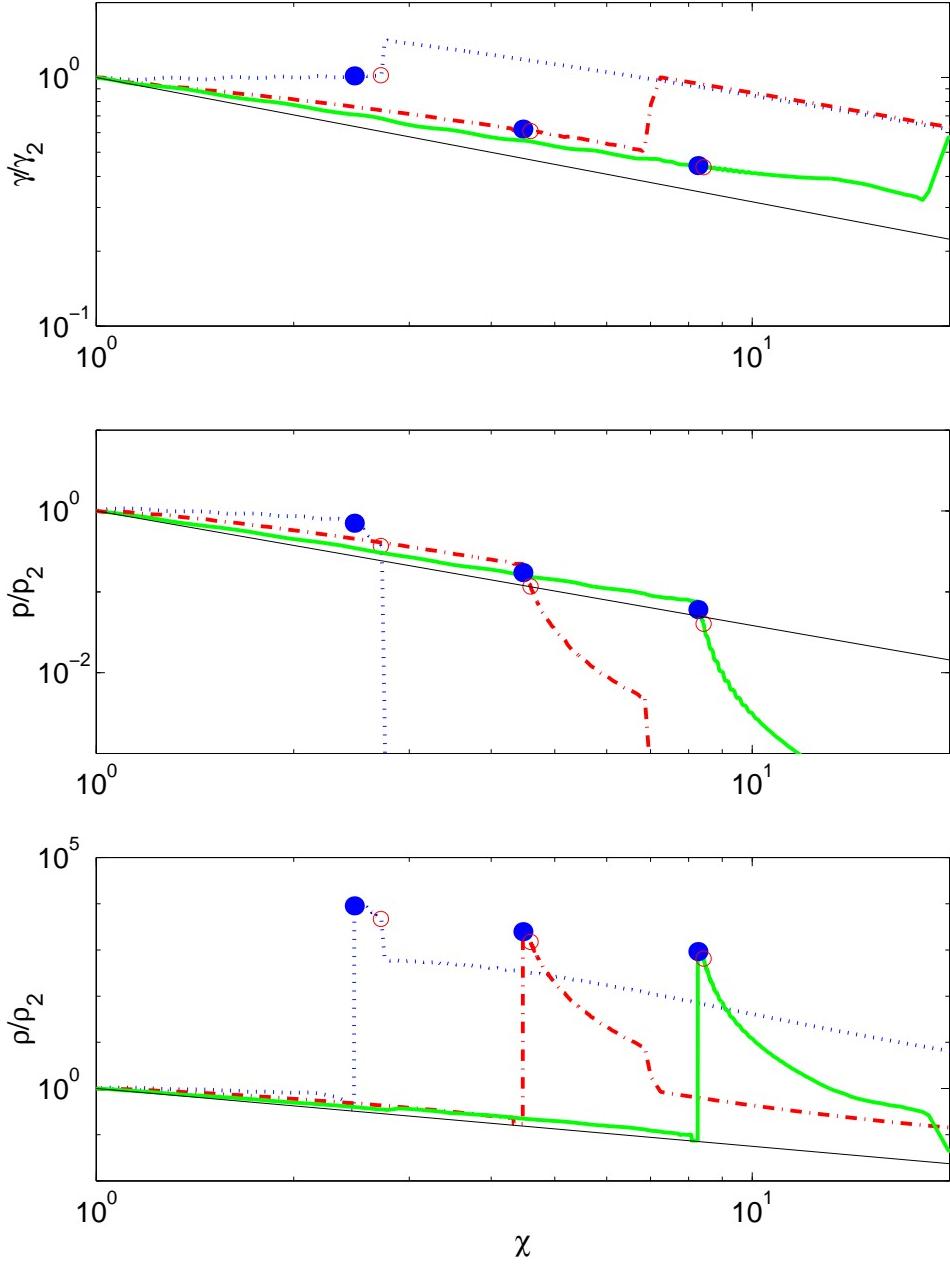
Fig. 6.— NRS case: Lorentz factor, pressure and density as functions of χ at $R_{\Delta,num}$ (dotted lines), at $2R_{\Delta,num}$ (dotted dashed lines) and at $3R_{\Delta,num}$ (solid lines). The Blandford-McKee solution is the thin solid lines.
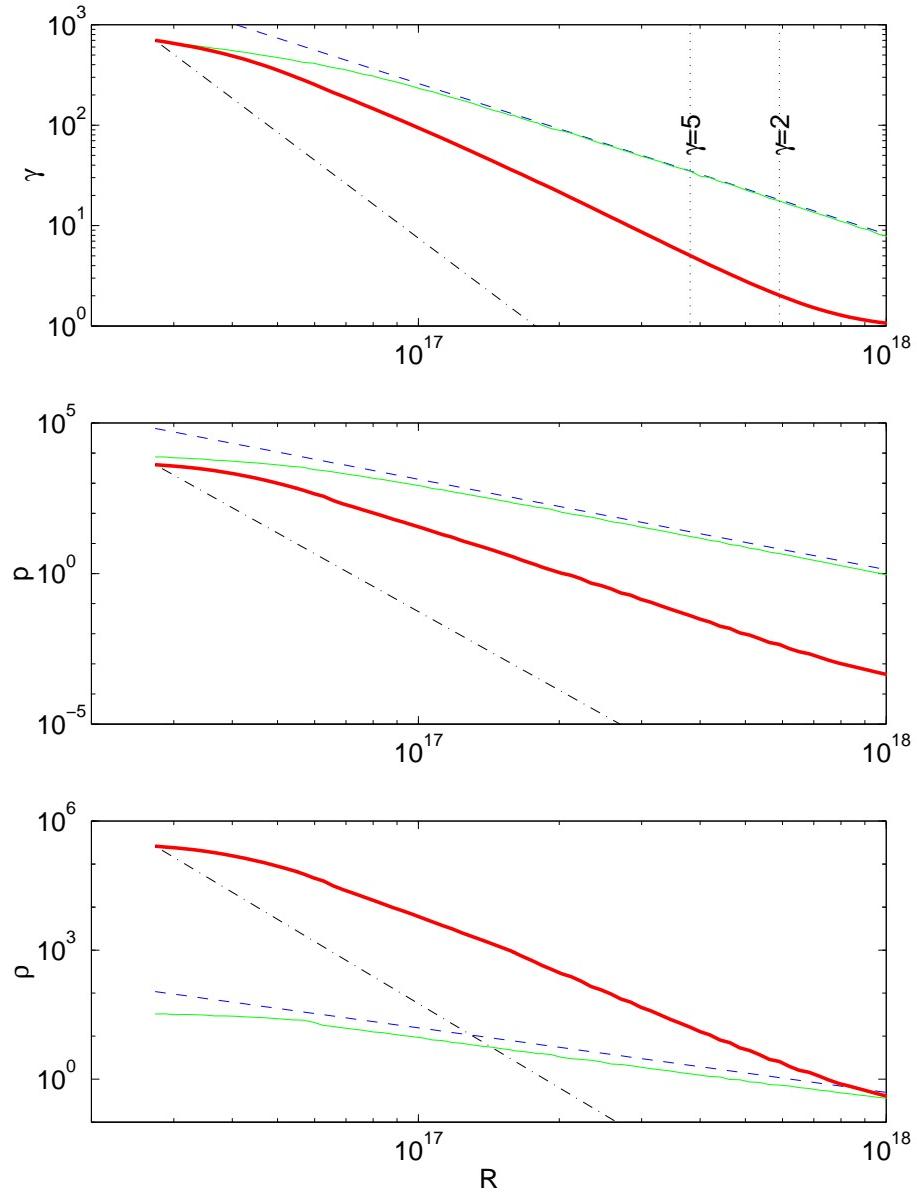
Fig. 7.— Evolution of Lorentz factor, pressure and density: NRS case. The numerical values just behind the forward shock are the thin solid lines, the expected values by the Blandford-McKee solution are the thin dashed lines. The numerical evolution of the averaged values in the ejecta shell (thick solid lines) are compared with the Blandford-McKee scalings of a fluid element (thin dashed dotted lines). The vertical dotted lines show the radius where the Lorentz factor of the ejecta is 2 or 5.
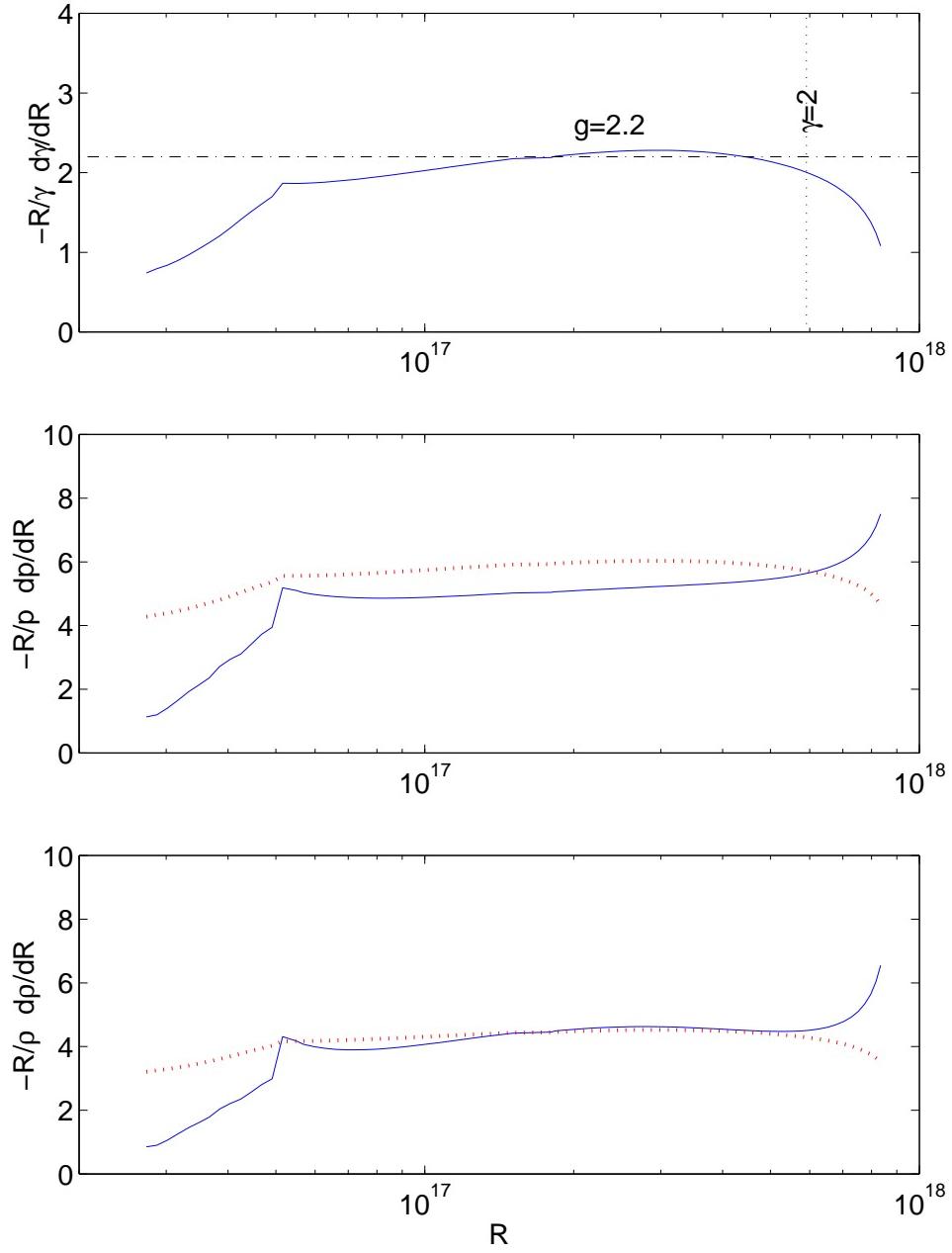
Fig. 8.— Effective scaling indexes vs Radius of the shell: NRS case. The numerical results are the solid lines. The dotted lines in the middle and the bottom panel are analytic estimates assuming the numerical index g.
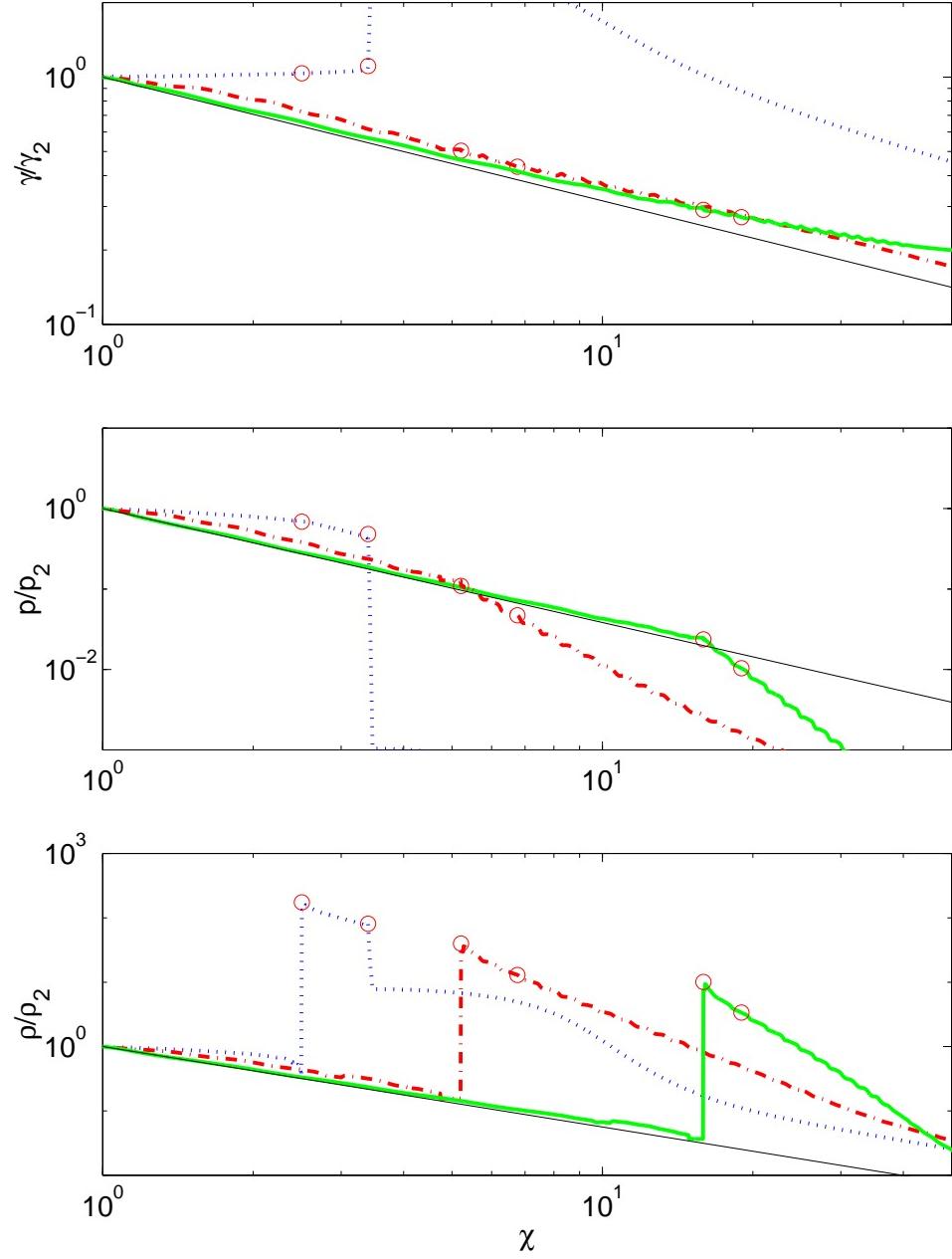
Fig. 9.— GRB990123: Lorentz factor, pressure and density as functions of χ at $R_{\Delta,num}$ (dotted lines), at $2R_{\Delta,num}$ (dotted dashed lines) and at $3R_{\Delta,num}$ (solid lines). The Blandford-McKee solution is the thin solid lines.
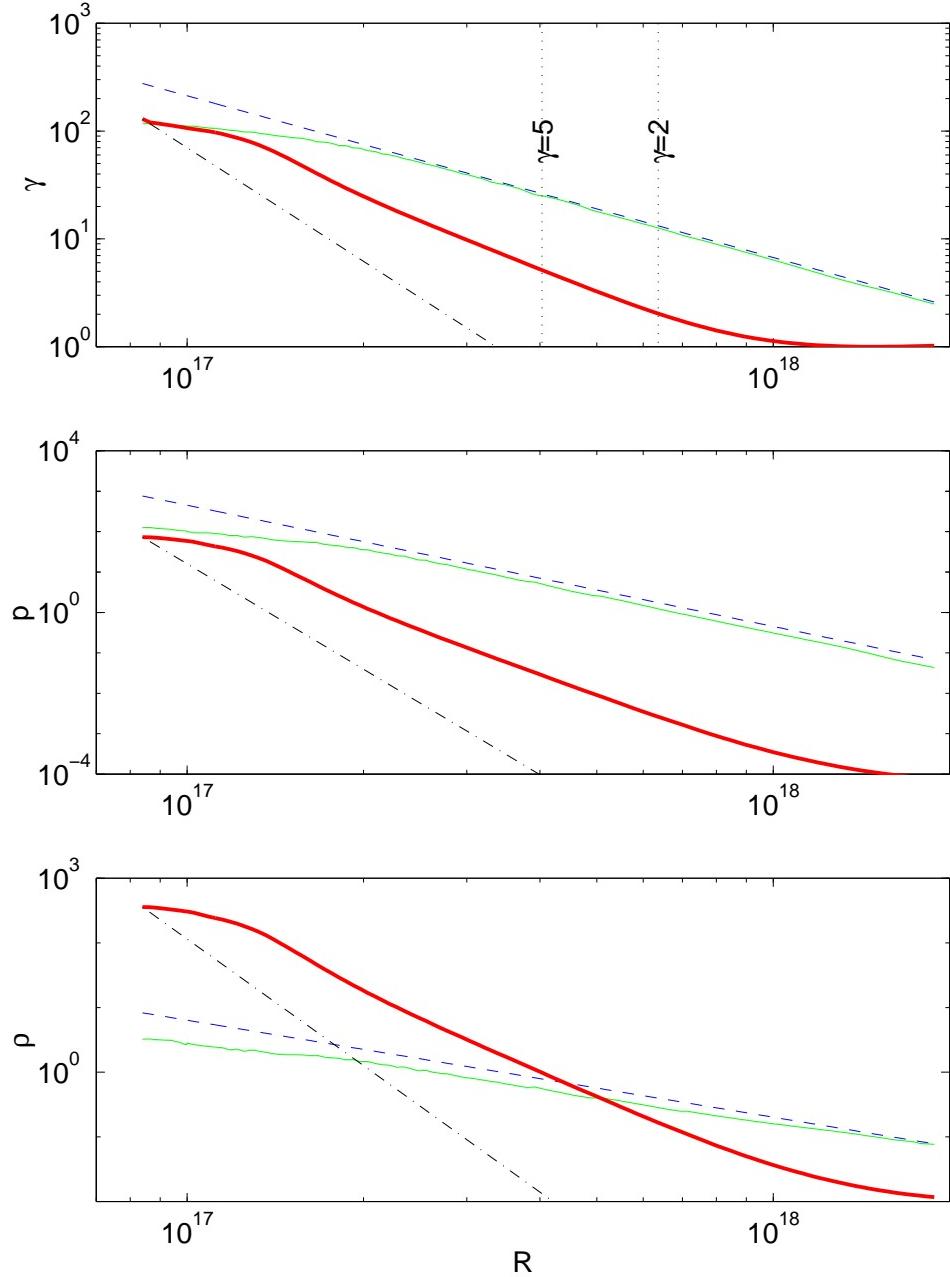
Fig. 10.— Evolution of Lorentz factor, pressure and density: GRB990123. Numerical values just behind the forward shock (thin solid), expected values by the Blandford-McKee solution (thin dashed). averaged values in the ejecta (thick solid lines) and the Blandford-McKee scalings of a fluid element (thin dashed dotted). The vertical dotted lines show the radius where the Lorentz factor of the ejecta is 2 or 5.
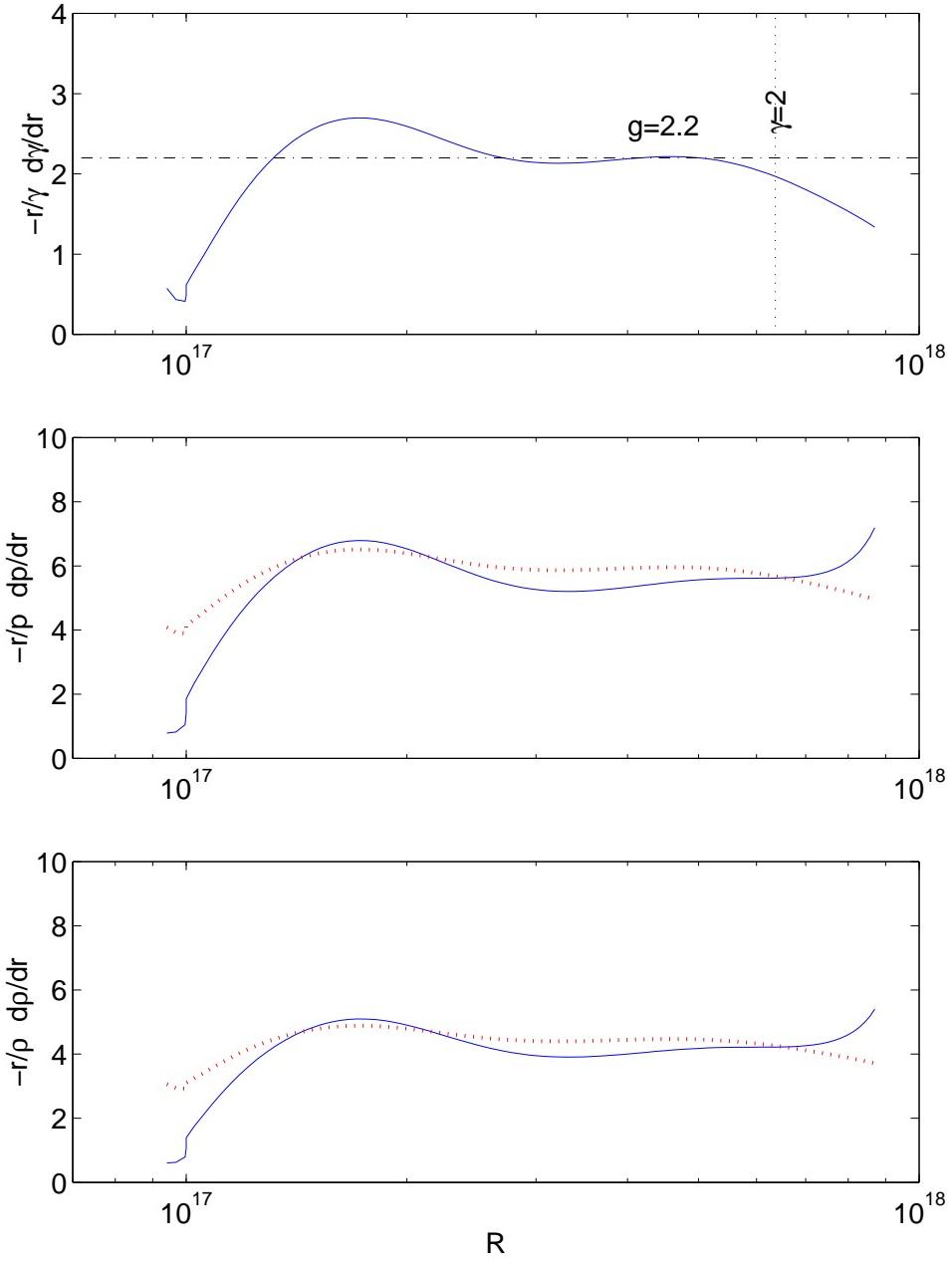
Fig. 11.— Effective scaling indexes vs Radius of the shell: GRB990123. The numerical results are the solid lines. The dotted lines in the middle and the bottom panel are analytic estimates assuming the numerical index g.
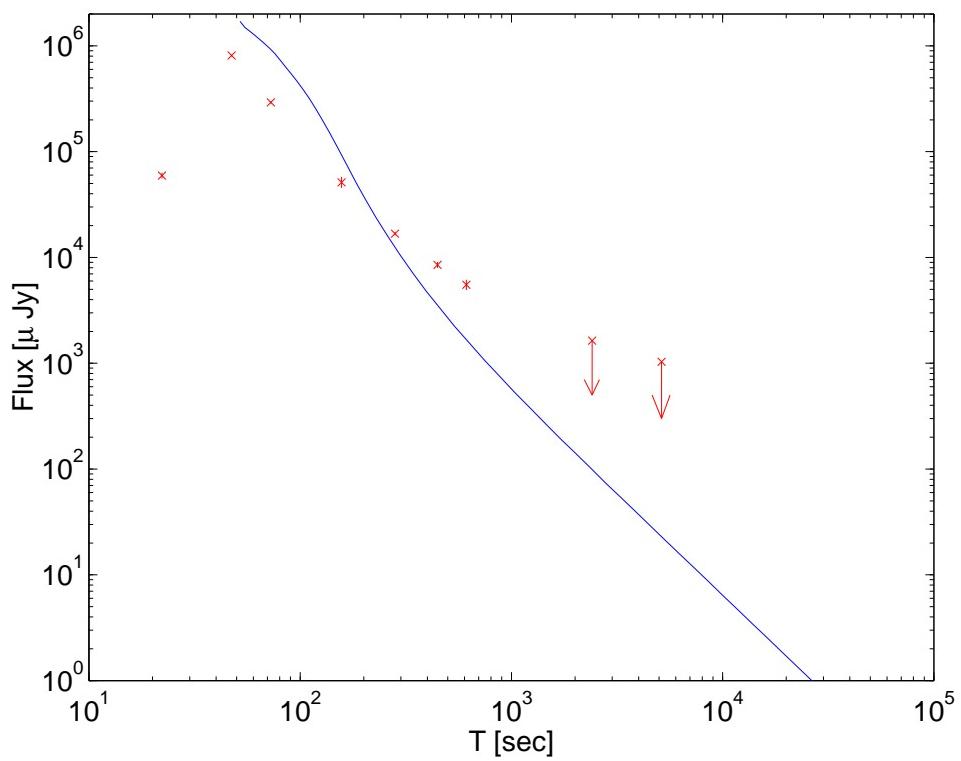
Fig. 12.— Optical light curve: GRB990123. The solid line depicts the numerical light curve. The stars are the ROTSE observations and the arrows show the upper limits.
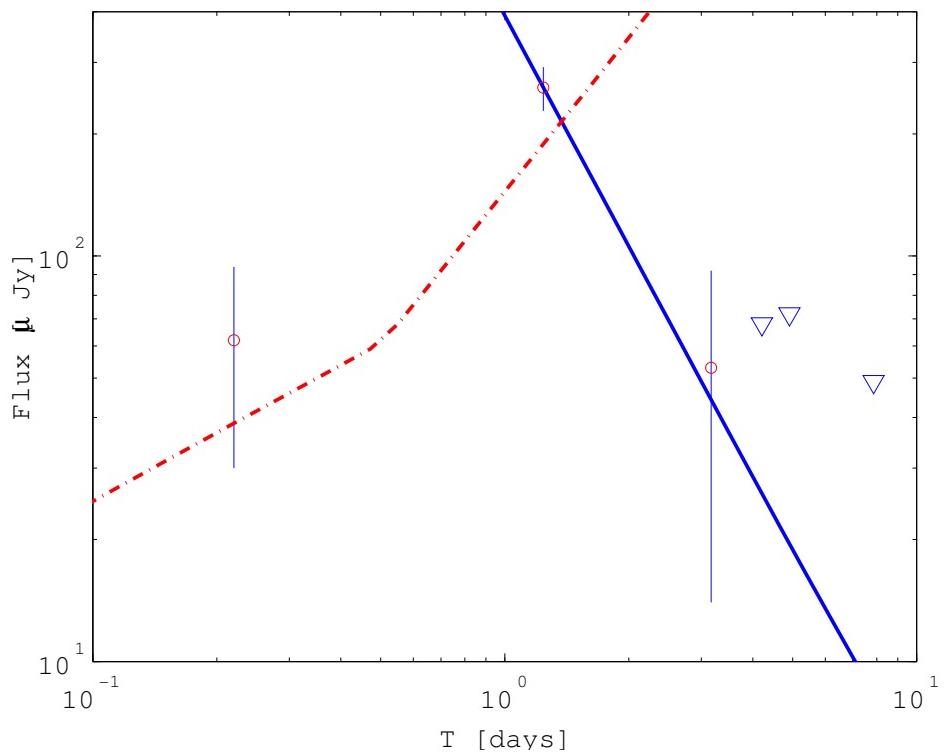
Fig. 13.— Radio light curve: GRB 990123. Numerical light curve (solid line), self absorption upper limit (dotted dashed line). Observations are also plotted, triangles are upper limits